Mon. Not. R. Astron. Soc. **000**, 000–000 (0000) Printed 31 October 2018 (MN LATEX style file v1.4)

Testing the Gaussianity of the COBE-DMR data with spherical wavelets

R.B. Barreiro[1], M.P. Hobson[1], A.N. Lasenby[1], A.J. Banday[2], K.M. Górski[3,4], and G. Hinshaw[5]

[1] *Astrophysics Group, Cavendish Laboratory, Madingley Road, Cambridge CB3 0HE, UK*
[2] *Max-Planck Institut fuer Astrophysik (MPA), Karl-Schwarzschild Str.1, D-85740, Garching, Germany*
[3] *European Southern Observatory (ESO), Karl-Schwarzschild Str.2, D-85740, Garching, Germany*
[4] *Warsaw University Observatory, Aleje Ujazdowskie 4, 00-478 Warszawa, Poland*
[5] *NASA/GSFC, Greenbelt, MD 20771, USA*

Accepted ???. Received ???; in original form ???

ABSTRACT

We investigate the Gaussianity of the 4-year COBE-DMR data (in HEALPix pixelisation) using an analysis based on spherical Haar wavelets. We use all the pixels lying outside the Galactic cut and compute the skewness, kurtosis and scale-scale correlation spectra for the wavelet coefficients at each scale. We also take into account the sensitivity of the method to the orientation of the input signal. We find a detection of non-Gaussianity at > 99 per cent level in just one of our statistics. Taking into account the total number of statistics computed, we estimate that the probability of obtaining such a detection by chance for an underlying Gaussian field is 0.69. Therefore, we conclude that the spherical wavelet technique shows no strong evidence of non-Gaussianity in the COBE-DMR data.

Key words: methods: data analysis-cosmic microwave background.

1 INTRODUCTION

The cosmic microwave background (CMB) provides a unique tool for investigating the formation of structure in the Universe. In particular, studying the Gaussianity of the CMB temperature fluctuations allows us to distinguish between two competing theories of structure formation: the standard inflationary model that predicts Gaussian fluctuations and topological defects that give rise to non-Gaussian signatures in the CMB. In order to test the Gaussianity of the CMB, a large number of methods have already been proposed in the literature (see e.g. Barreiro 2000 and references therein). In particular, many of them have been applied to the 4-year COBE-DMR data, although most have not yielded any detection of non-Gaussianity (see e.g. Mukherjee, Hobson & Lasenby 2000).

Nevertheless, three apparently robust detections of non-Gaussianity in the 4-year COBE-DMR data have recently been reported. Ferreira, Magueijo & Górski (1998) studied the distribution of an estimator for the normalised bispectrum, finding that Gaussianity is ruled out at the 98 per cent confidence level with the non-Gaussian signal mainly concentrated on the multipole $l = 16$. Although this non-Gaussian signal is certainly present in the data, Banday, Zaroubi & Górski (1999) have shown in a recent work that this non-Gaussian signal is most probably due to a systematic artefact. However, Magueijo (1999) has found a new non-Gaussian signal above the 97 per cent confidence level using an extended bispectrum analysis, which is present even when the artefacts found by Banday et al. are removed.

Complementary to the above bispectrum analysis, Pando, Valls-Gabaud & Fang (1998) applied a technique based on the discrete wavelet transform to Face 0 and Face 5 of the QuadCube pixelisation of COBE-DMR data. On computing the scale-scale correlations of the wavelet coefficients in certain domains of the wavelet transform, they found a significant non-Gaussian signal at the 99 per cent confidence level in Face 0 corresponding to scales of $11 - 22$ degrees. However, no significant deviation from Gaussianity was found using the skewness and kurtosis of the wavelet coefficients at each of the considered domains. Mukherjee, Hobson & Lasenby (2000) (hereinafter MHL) have recently revised the previous work, taking into account that a large number of the computed statistics show no evidence of non-Gaussianity, and pointing out that the results depend critically on the orientation of the data. They find that Gaussianity can only be ruled out at the 41 per cent confidence level in the DSMB data and at the 72 per cent level in the 53+90 GHz coadded data and therefore that this analysis does not provide strong evidence for non-Gaussianity in the COBE-DMR data.

The above wavelet analyses were performed by applying planar (Daubechies) wavelets to Face 0 and Face 5 of the COBE-DMR QuadCube pixelisation in Galactic coordinates (i.e. the faces centred on the North and South Galactic poles respectively). This procedure thus uses only one-third of the COBE-DMR data and, furthermore, can lead to distortions of the CMB fluctuations when moving from the sphere to the planar faces of the QuadCube. Therefore, in this paper, we use orthogonal spherical Haar wavelets (SHW) (Girardi & Sweldens 1995, Sweldens 1995), which are better suited to analysing data over large regions of the sky (such as the COBE-DMR maps). These wavelets were introduced as a generalisation of planar Haar wavelets to more general spaces than R^n. Indeed, Tenorio et al. (1999) have used SHW as a tool for studying the spatial structure, denoising and compression of CMB maps. We use SHW to perform a similar analysis to those of Pando et al and MHL, based on the skewness, kurtosis and scale-scale correlation of the wavelet coefficients, in order to search for evidence of non-Gaussianity in the 4-year COBE-DMR data. A hierarchical pixelisation scheme which is particularly well-suited to the application of such a wavelet decomposition is HEALPix (Górski, Hivon & Wandelt 1999). Therefore, we apply the former analysis to the COBE-DMR data in HEALPix pixelisation (Banday et al. 2000). We also include a Galactic cut derived by a simple propagation of the customised Galactic cut of Banday et al. (1997) and Bennett et al. (1996) to the HEALPix pixelisation. Owing to the characteristics of the SHW transform, it is straightforward to use *all* the pixels lying outside the Galactic cut, which constitutes approximately two-thirds of the total number of COBE-DMR pixels.

2 THE WAVELET ANALYSIS

2.1 Spherical Haar Wavelets

Orthogonal SHW are an example of the so-called 'second generation wavelets' (Sweldens 1995, Schroeder & Sweldens 1995). These wavelets are not dilations and translations of a given function and can therefore be adapted to more general spaces than R^n but, at the same time, they still enjoy all the useful properties of planar wavelets, such as good space-frequency localisation and a fast transform algorithm.

The temperature field can be decomposed into the SHW basis functions:

$$\frac{\Delta T}{T}(x_i) = \sum_{l=0}^{n_{j_0}-1} \lambda_{j_0,l}\varphi_{j_0,l}(x_i) + \sum_{m}\sum_{j=j_0}^{J-1}\sum_{l=0}^{n_j-1} \gamma_{m,j,l}\psi_{m,j,l}(x_i) \quad (1)$$

where $\lambda_{j_0,l}$ and $\gamma_{m,j,l}$ are the approximation and detail wavelet coefficients respectively. The first term in (1) corresponds to a smoother image of the original map, whereas the detail coefficients encode the differences between the smoothed map and the original. The index j runs over the different scales, with J being the resolution of the original map and j_0 the coarsest resolution considered. n_j is the number of pixels at resolution j. Finally, the index m corresponds to the number of different wavelet functions at each scale required in order to form a complete orthogonal basis set. In particular, for a square partitioning, such as that in the HEALPix pixelisation, we require three different wavelet basis functions at each scale j, and therefore we have three different kind of wavelet coefficients $\gamma_{1,j,l}$, $\gamma_{2,j,l}$ and $\gamma_{3,j,l}$. A more detailed description of the SHW transform is given in Appendix A.

As pointed out by MHL, we note that the asymmetry of orthogonal wavelet basis functions means that the wavelet decomposition is sensitive to the orientation of the input signal. Thus any statistics based on the corresponding wavelet coefficients are also sensitive to the orientation of the analysed signal.

Figure 1. In the top figure, the coadded 53+90 GHz COBE-DMR map in HEALPix pixelisation at resolution $J = 7$ with the customised Galactic cut is plotted. The bottom map shows the twelve pixels of the base-resolution of HEALPix ($j = 1$) and how they are affected by such a cut.

2.2 Application to COBE-DMR data

In this paper, we analyse the 4-year COBE-DMR data in HEALPix pixelisation. A detailed description of the process of map-making is given by Banday et al. (2000). HEALPix is an equal area, iso-latitude and hierarchical pixelisation of the sphere. The base-resolution comprises twelve pixels in three rings around the poles and equator (see Fig. 1). The resolution level of the grid is expressed by the parameter $N_{\rm side}$, that indicates the number of divisions along the side of the base-resolution pixel that is needed to reach a desired high-resolution partition. For convenience we will use instead the index j to refer to the scale; this relates to $N_{\rm side}$ as $N_{\rm side} = 2^{j-1}$.

In the case of the COBE-DMR maps, the total number of pixels is 49152 (i.e. $J = 7$, or equivalently $N_{\rm side} = 64$), with a pixel linear size of $\simeq 55'$. Therefore, each resolution level j corresponds to a scale $55' \times 2^{J-j}$, containing $n_j = 12 \times 4^{j-1}$ pixels of that size.

We have used in our analysis the coadded 53A, 53B, 90A and 90B map (each pixel weighted according to the inverse of its noise variance) with the customised Galactic cut, which is plotted in Fig. 1 (Banday et al. 2000, Banday et al. 1997, Bennett et al. 1996). As mentioned above, we are thus using approximately two-thirds of the data as opposed to previous analyses that kept only one-third (Face 0 and Face 5) of the QuadCube COBE-DMR data. In addition, we avoid any possible projection effects in going from the sphere to the cube.

2.3 The non-Gaussianity test

In our wavelet analysis we have considered separately the detail coefficients corresponding to $m = 1, 2, 3$ at each scale j. For each value of j and m, we use the corresponding detail coefficients $\gamma_{m,j,l}$ to estimate the skewness $\hat{S}$ and (excess) kurtosis $\hat{K}$ of the parent distribution from which the coefficients were drawn. We therefore obtain the skewness $\hat{S}(j,m)$ and kurtosis $\hat{K}(j,m)$ spectra for the image. At each value

(j,m), the skewness and kurtosis of the parent distribution of the wavelet coefficients is given by

$$S = \kappa_3/\kappa_2^{3/2} \tag{2}$$

$$K = \kappa_4/\kappa_2^2 \tag{3}$$

where κ_n is the nth cumulant of the distribution. Following Hobson, Jones & Lasenby (1999) we use k-statistics (see Kenney & Keeping 1954; Stuart & Ord 1994) to obtain unbiased estimators of the cumulants, which are then used to estimate the skewness $\hat{S}$ and (excess) kurtosis $\hat{K}$.

In addition to the skewness and kurtosis spectra, we measure the scale-scale correlation between the wavelet coefficients at different scales using the following estimator:

$$\hat{C}^p(j,m) = \frac{n_{j+1}\sum_{l=0}^{n_{j+1}-1}\gamma^p_{m,j,[l/4]}\gamma^p_{m,j+1,l}}{\sum_{l=0}^{n_{j+1}-1}\gamma^p_{m,j,[l/4]}\sum_{l=0}^{n_{j+1}-1}\gamma^p_{m,j+1,l}} \tag{4}$$

where [ ] denotes the integer part and $n_j = 12\times 4^{j-1}$ is the number of pixels at the resolution level j. The scale-scale correlation coefficient $\hat{C}^p(j,m)$ measures the correlation between each type of detail coefficient γ (i.e. for $m=1,2,3$) in the two consecutive scales j and $j+1$. We restrict our analysis to the case $p=2$.

In our non-Gaussianity test, we first obtain the skewness, kurtosis and scale-scale correlation spectra for the coadded 53+90 GHz COBE-DMR map. Those wavelet coefficients sensitive to pixels inside the Galactic cut are not used in the computations. We then generate 10000 realisations of CMB all-sky maps, smoothed with a 7° Gaussian beam, and add levels of Gaussian noise corresponding to the COBE-DMR data. The CMB maps are drawn from an inflationary/CDM model with parameters $\Omega_m = 1$, $\Omega_\Lambda = 0$, $h = 0.5$, $n = 1$ and $Q_{rms-ps} = 18\mu K$, but we do not expect our analysis to be very sensitive to a difference choice of parameters (see MHL). We then compute our estimators for each of the CDM simulations to obtain approximate probability distributions for the $\hat{S}(j,m)$, $\hat{K}(j,m)$ and $\hat{C}^2(j,m)$ statistics for a CMB signal derived from the chosen model. By comparing these distributions with the values obtained from the COBE-DMR data, we can obtain the probability that our data are derived from a Gaussian distribution characterised by the chosen power spectrum.

For each kind of detail coefficient ($m=1,2,3$), we calculate the skewness and kurtosis at five different scales, and also calculate four scale-scale correlation coefficients. Therefore we compute a total of 42 different statistics, which must be taken into account when assigning a statistical significance to a given detection. In addition, as we have already discussed, this wavelet decomposition is sensitive to the orientation of the data. Therefore, we perform the entire test for three different orientations of the COBE-DMR map.

3 RESULTS

The computed $\hat{S}(j,m)$, $\hat{K}(j,m)$ and $\hat{C}^2(j,m)$ spectra are plotted in Fig. 2 for three different orientations. We rotate the 53+90 COBE-DMR map around an axis passing through the North and South Galactic poles. Due to the characteristics of the HEALPix pixelisation, a rotation in this direction of 90 degrees simply shifts the twelve base-pixels into each other, and thus recovers the original result. Therefore, we show the results computed from the COBE-DMR data for a rotation of 0 (orientation A, solid squares), 30 (orientation B, crosses) and 60 (orientation C, stars) degrees with respect to the original orientation of the 53+90 COBE-DMR map. The open circle corresponds to the average over 10000 CDM simulations generated as explained before and the error bars indicate the 68, 95 and 99 per cent confidence levels of the distributions for orientation A. Note that for convenience the $K(j,m)$ and $S(j,m)$ spectra have been normalised at each value of (j,m) such that the variance of the distribution obtained from the 10000 CDM realisations is equal to unity. We do not plot the corresponding error bars for orientations B and C in Fig. 2 for the sake of clarity and because the conclusions derived from the plot remain unchanged. In fact, due to the isotropy of the CMB, we expect these error distributions to be independent of the chosen orientation, although small variations do appear (see Fig. 3) due to the presence of anisotropic noise and as a consequence of having a pixelised map.

We see from Fig. 2 that for orientation A (solid squares) all the points of skewness and scale-scale correlation spectra lie within their respective Gaussian probability distributions. However, we find a detection of non-Gaussianity at a confidence level > 99 per cent for the kurtosis at $j=2$, $m=3$. On the other hand, for orientations B (crosses) and C (stars) all the COBE-DMR values are consistent with being derived from a parent Gaussian distribution.

We must be careful when assessing the significance of the non-Gaussian detection for orientation A. We must take into account that we have computed a total of $3\times 42 = 126$ different statistics and most of them show no evidence of non-Gaussianity (see Bromley & Tegmark 1999). Following MHL, since the different statistics are not independent, we must use Monte-Carlo simulations to estimate the probability of having at least one detection of non-Gaussianity when computing these 126 statistics at a confidence level > 99 per cent even in the case of an underlying Gaussian signal. We find that this occurs in 69 per cent of the cases. Therefore this analysis does not provide strong evidence of non-Gaussianity, in agreement with the results obtained by MHL using planar wavelets.

We may wonder, however, if our conclusions are affected by choosing a different set of orientations for the COBE-DMR maps. As an illustration of the sensitivity of the computed statistics to the orientation of the data, Fig. 3 shows $\hat{S}(j,m)$,$\hat{K}(j,m)$ and $\hat{C^2}(j,m)$ for $m=2$ and two different scales versus the angle that the COBE-DMR data have been rotated around an axis passing through the North and South Galactic poles with respect to the original signal. The average value and the 68, 95 and 99 per cent confidence levels obtained from the corresponding Gaussian distributions are also plotted for orientations A,B and C. Note that, in this case, the skewness and kurtosis spectra has *not* been normalised as in Fig. 2. It can be seen that the COBE-DMR values of the skewness, kurtosis and scale-scale correlation at each scale oscillate around the mean obtained from the CDM realisations and with a deviation in agreement with the confidence limits showed for orientations A,B and C. We have also checked that, as expected, we obtain very similar variations when rotations are performed around different directions. Therefore, although the particular numerical values of the considered statistics are not rotationally invariant, the

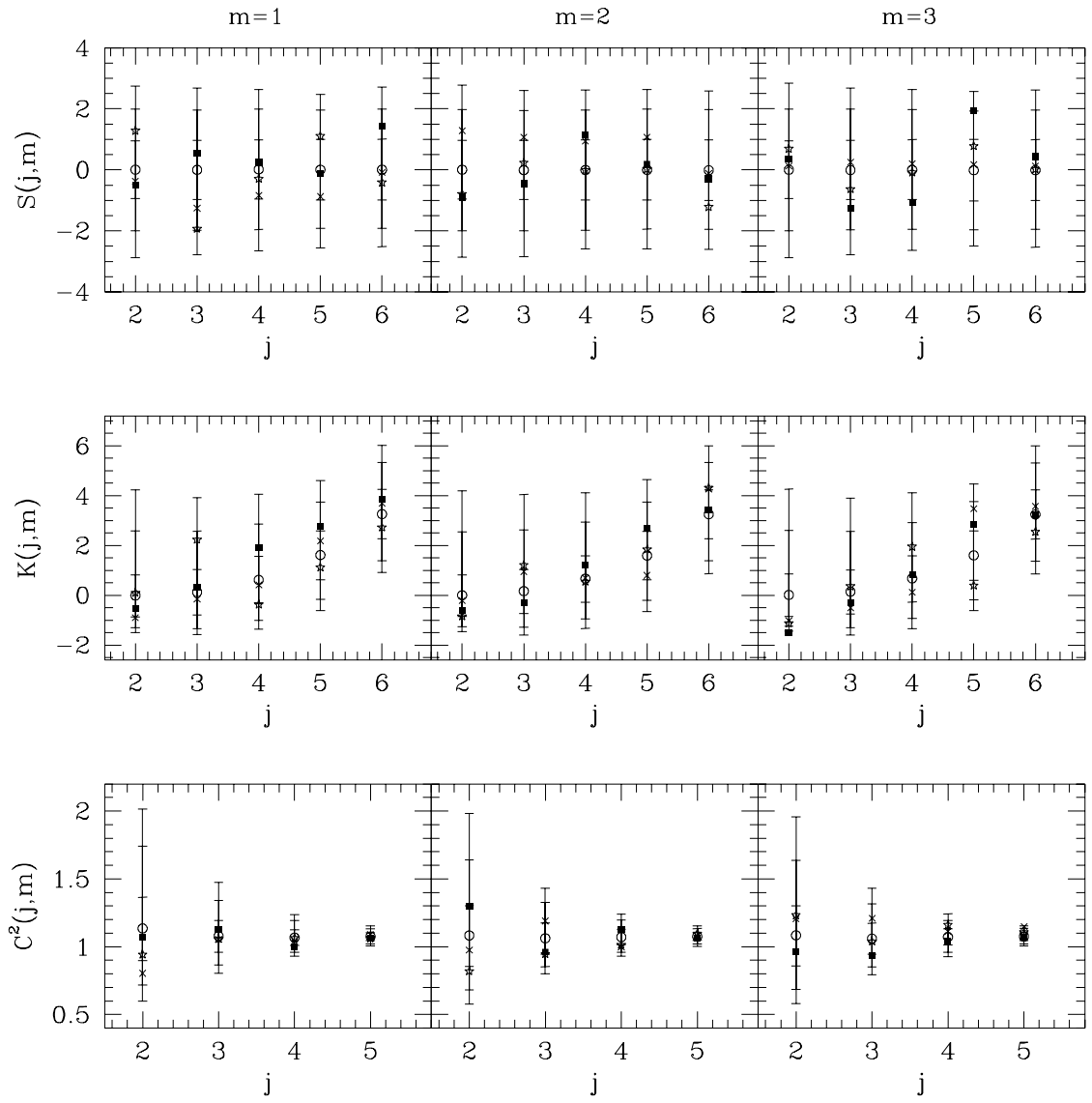

Figure 2. The skewness, kurtosis and scale-scale correlation spectra for the 53+90 GHz COBE-DMR map are plotted for each type of detail coefficient $m = 1$ (first column), $m = 2$ (second column) and $m = 3$ (third column). Solid squares, crosses and stars correspond respectively to the the data rotated 0, 30 and 60 degrees around an axis passing through the North and South Galactic poles with respect to the input signal (orientations A, B and C). The error bars denote the 68, 95 and 99 per cent limits of the corresponding distribution. For convenience, $\hat{S}(j,m)$ and $\hat{K}(j,m)$ have been normalised at each value of (j,m) such that the variance of the distribution obtained from the 10000 CDM realisations is equal to unity

general conclusions concerning non-Gaussianity of the data, at least in our case, do not seem to depend on the chosen orientation.

4 CONCLUSIONS

We presented an analysis of the 4-year COBE-DMR data (in HEALPix pixelisation) based on spherical Haar wavelets (SHW) in order to look for large scale non-Gaussianity of the CMB. This analysis is performed using all the available data lying outside the Galactic cut. This constitutes about two-thirds of the pixels, as compared to just one-third in former works that use only Face 0 and Face 5 of the Quad-Cube pixelisation. We take into account the sensitivity of the method to the orientation of the original signal and present the results for three different orientations of the data. We also find that the choice of a different set of orientations, at least in our case, does not alter the general conclusions regarding non-Gaussianity.

We find that the value of the kurtosis for $j = 2, m = 3$ for one of the chosen orientations lies outside the 99 per cent confidence level derived from 10000 CDM/inflationary realisations, whereas the rest of the statistics show no evidence of non-Gaussianity. However, since we have a total

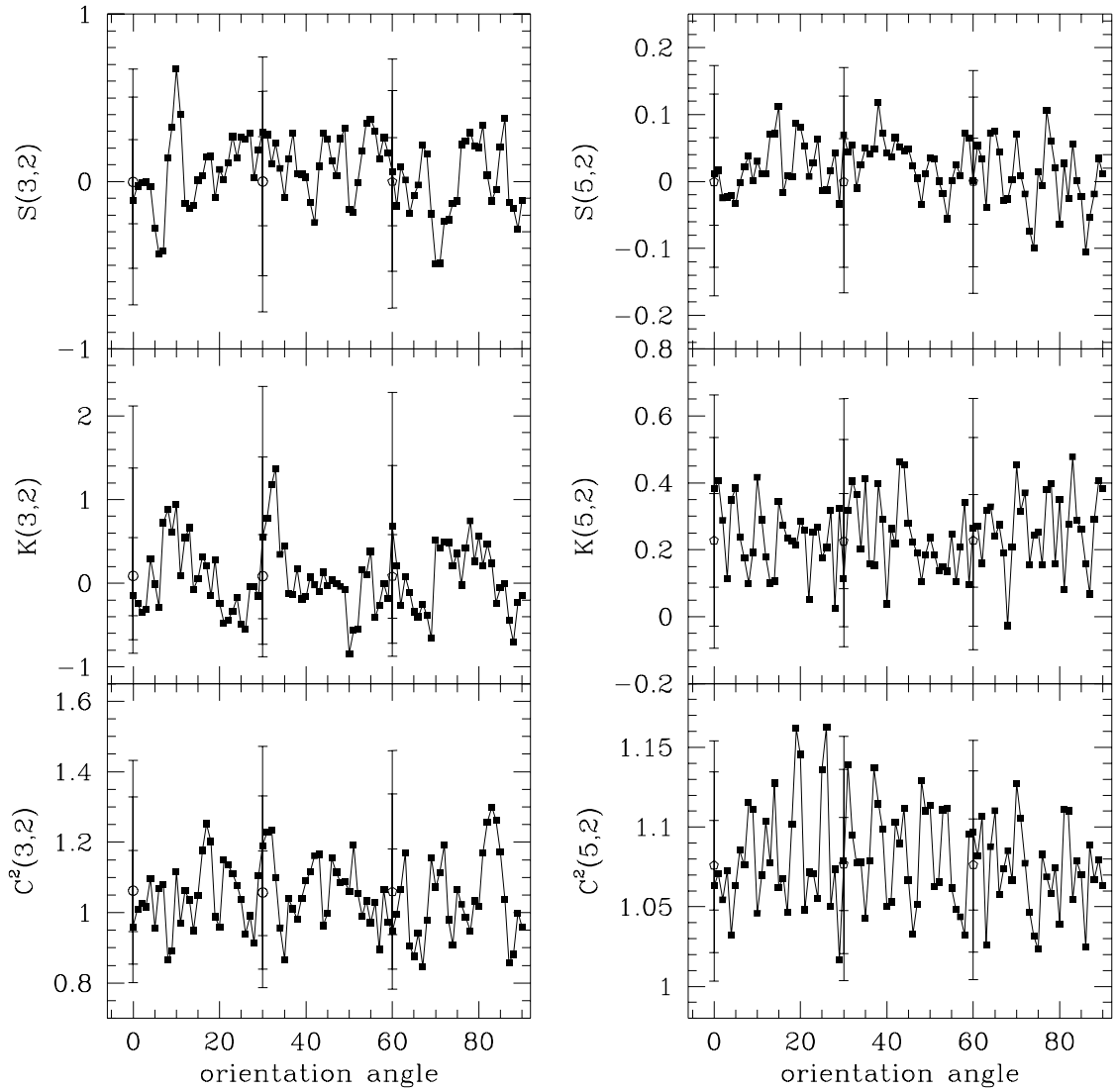

Figure 3. The $\hat{S}(j,m)$,$\hat{K}(j,m)$ and $\hat{C^2}(j,m)$ spectra are shown for values of $j = 3, 5$ and $m = 2$ versus the angle that the COBE-DMR data have been rotated around an axis passing through the North and South Galactic poles with respect to the original signal. The average value and the 68, 95 and 99 per cent confidence levels obtained from the corresponding Gaussian distributions are also plotted for values of the orientation angle equal to 0, 30 and 60 degrees (orientations A, B and C, respectively). Note that the skewness and kurtosis spectra have *not* been normalised as in Fig. 2

of 126 different statistics, the probability of finding at least one of them falling outside the 99 per cent confidence level even in the case of an underlying Gaussian field is as high as 0.69. Therefore, we conclude that an analysis based on SHW of the 4-year COBE-DMR data show no evidence for non-Gaussianity.

ACKNOWLEDGEMENTS

RBB warmly thanks Luis Tenorio for helpful comments about spherical wavelets. We thank all the people involved in the HEALPix collaboration (Górski, Hivon & Wandelt 1999), whose package has been used extensively in this work. RBB and MPH acknowledge financial support from the PPARC in the form of a research grant and an Advanced Fellowship respectively. ANL acknowledges support from the Royal Society and Leverhulme Trust.

REFERENCES

Banday A.J. et al., 2000, in preparation
Banday A.J., Górski K.M., Bennett C.L., Hinshaw G., Kogut A., Lineweaver C., Smoot G.F., Tenorio L., 1997, ApJ, 475, 393
Banday A.J., Zaroubi S., Górski K.M., 2000, ApJ, in press (astro-ph/9908070)
Barreiro R.B., 2000, New Astr.Rev., in press (astro-ph/9907094)

Bennett C.L. et al., 1996, ApJ, 464, L1
Bromley C.L., Tegmark M., 1999, ApJ, 524, L79
Ferreira P., Magueijo J., Górski K.M., 1998, ApJ, 503, L1
Girardi M., Sweldens W., 1995, Technical Report, University of South Carolina
Górski K.M., Hivon E., Wandelt B.D., 1999, in 'Evolution of Large-Scale Structure: from Recombination to Garching', p.37, PrintPartners Ipskamp; http://www.tac.dk/∼healpix
Hobson M.P., Jones A.W., Lasenby A.N., 1999, MNRAS, 309, 125
Kenney J.F., Keeping E.S., 1954, Mathematics of Statistics (Part I). Van Nostrand, New York
Magueijo J., 2000, ApJ, 528, L57 (see also Magueijo J., 2000, ApJ, 532, L157)
Mukherjee P., Hobson M.P., Lasenby A.N., 2000, MNRAS, in press (astro-ph/0001385)(MHL)
Pando J., Valls-Gabaud D., Fang L.-Z., 1998, Phys.Rev.Lett., 81, 4568
Schroeder P., Sweldens W., 1995, Technical Report, University of South Carolina
Stuart A., Ord K.J., 1994, Kendall's Advanced Theory of Statistics (Volume I). Edward Arnold, London
Sweldens W., 1995, Technical Report, University of South Carolina
Tenorio L., Jaffe A.H., Hanany S., Lineweaver C.H., 1999, MNRAS, 310, 823

APPENDIX A: SPERICAL HAAR WAVELETS FOR HEALPix PIXELISATION

In this Appendix, we give an heuristic approach to decomposing a map in HEALPix pixelisation in terms of spherical Haar wavelet coefficients. More mathematical approaches are given elsewhere (Sweldens 1995).

HEALPix is an equal area, iso-latitude and hierarchical pixelisation of the sphere. The resolution level of the grid is given by the parameter j (or equivalently $N_{\rm side}$, $N_{\rm side} = 2^{j-1}$). A level j comprises a total of $n_j = 12 \times 4^{j-1}$ pixels, each of them with equal area μ_j. Each pixel l at resolution j, $S_{j,l}$, is divided into four pixels $S_{j+1,l_0}, ..., S_{j+1,l_3}$ at resolution $j+1$. In particular, the COBE-DMR resolution corresponds to $J = 7$.

In order to perform a SHW decomposition of the COBE-DMR data, we require one scaling $\varphi_{j,l}$ and three wavelet functions $\psi_{m,j,l}$ at each scale j and position l. These are given by

$$\varphi_{j,l}(x) = \begin{cases} 1, & \text{if } x \epsilon S_{j,l} \\ 0, & \text{otherwise} \end{cases} \tag{A1}$$

$$\psi_{1,j,l} = \frac{\varphi_{j+1,l_0} + \varphi_{j+1,l_2} - (\varphi_{j+1,l_1} + \varphi_{j+1,l_3})}{4\mu_{j+1}} \tag{A2}$$

$$\psi_{2,j,l} = \frac{1}{2\mu_{j+1}} (\varphi_{j+1,l_1} - \varphi_{j+1,l_3}) \tag{A3}$$

$$\psi_{3,j,l} = \frac{1}{2\mu_{j+1}} (\varphi_{j+1,l_0} - \varphi_{j+1,l_2}) \tag{A4}$$

where l_0, l_1, l_2, l_3 are the four pixels at resolution level $j+1$ contained within the pixel l at level j, and we have taken into account that all pixels have equal area at a given resolution. The orthogonality of the wavelet functions follows immediately from their vanishing integral (by construction) and their support. The temperature field $\Delta T/T$ on the sphere can then be written as

$$\frac{\Delta T}{T}(x_i) = \sum_{l=0}^{n_{j_0}-1} \lambda_{j_0,l} \varphi_{j_0,l}(x_i) + \sum_{m=1}^{3} \sum_{j=j_0}^{J-1} \sum_{l=0}^{n_j-1} \gamma_{m,j,l} \psi_{m,j,l}(x_i) \tag{A5}$$

where $\lambda_{j_0,l}$ and $\gamma_{m,j,l}$ are the approximation and detail wavelet coefficients respectively. The index j runs over the different scales with J the resolution of the original map and j_0 the coarsest resolution considered.

The procedure to obtain the wavelet coefficients is as follows (see Fig A1). We start with a map at a resolution J, identifying each pixel with the $\lambda_{J,l}$ coefficients. Each approximation and detail coefficient at position l and resolution level $J-1$ is obtained as a linear combination of the four corresponding pixels l_0,l_1,l_2,l_3 at resolution J:

$$\lambda_{J-1,l} = \frac{1}{4} \sum_{i=0}^{3} \lambda_{J,l_i} \tag{A6}$$

$$\gamma_{m,J-1,l} = \sum_{i=0}^{3} \tilde{g}_{m,J-1,l_i} \lambda_{J,l_i} \tag{A7}$$

The approximation coefficients at the new resolution level are just the average over the four original coefficients and, therefore, correspond to a lower resolution version of the initial image. Complementary to those, the details encode the difference between the degraded and the original maps. The $\tilde{g}_{m,j,l}$ coefficients take values $+\mu_{j+1}$, $-\mu_{j-1}$ or 0, depend-

Figure A1. The COBE-DMR map in HEALPix pixelisation at resolution $J = 7$ and the wavelet coefficients at $j = 6$ are shown. Starting from the coefficients at the highest resolution J, the approximation and detail coefficients at $J-1$ are obtained as linear combinations of the original image (as shown in Fig A2). The process is repeated over the map formed by the $\lambda_{J-1,l}$ coefficients and so on down to the lowest resolution considered j_0.

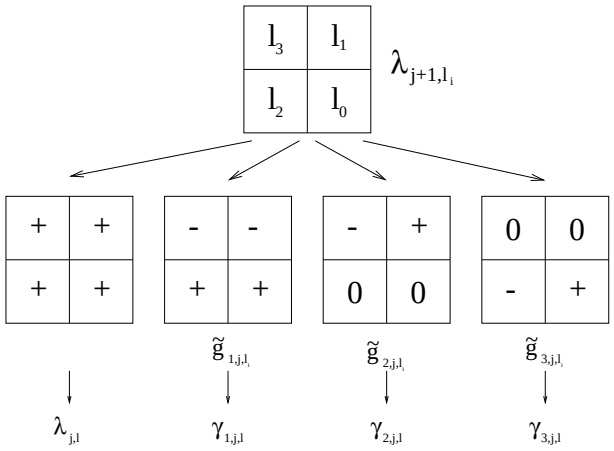

Figure A2. The procedure to obtain the wavelet coefficients at a resolution level j is shown. Each coefficient is obtained from a linear combination of four approximation coefficients at the level $j+1$. The new λ_j, l are just the average over the four original ones. The value of the $\tilde{g}_{m,j,l_i}$ factors used to obtain the details is $+\mu_{j+1}$, $-\mu_{j+1}$ or 0 as indicated in the figure.

ing on the indices, as shown in Fig. A2. These coefficients are obtained as an integral over the dual function of $\psi_{m,j,l}$ in the corresponding support (see e.g. Tenorio et al. 1999). Therefore, at level $J-1$ we have three different sets of details and one set of approximation coefficients, each of them with $n_{J-1} = n_J/4$ pixels.

Then, we apply the same procedure to the degraded map formed by $\lambda_{J-1,l}$, obtaining again a coarser image and a set of details corresponding to the resolution level $J-2$. Repeating this process down to the lowest resolution considered in our analysis, j_0, we are left with the details for resolutions $J-1$ to j_0 as well as the approximation λ_{j_0} coefficients. With this scheme it is also straightforward to identify those coefficients which are descendants of pixels contaminated by the Galaxy and discard them when performing the analysis.

To recover the map we just need to invert the process, starting with the approximation and detail coefficients at the lowest resolution j_0 up to the map at the initial resolution J.

This figure "cobeshw.jpg" is available in "jpg" format from:

http://arxiv.org/ps/astro-ph/0004202v1

This figure "cut.gif" is available in "gif" format from:

http://arxiv.org/ps/astro-ph/0004202v1

This figure "sky53ab_90ab_nest_tt_cut.gif" is available in "gif" format from:

http://arxiv.org/ps/astro-ph/0004202v1